FIRST RESULTS FROM VIRGO, THE EXPERIMENT FOR HELIOSEISMOLOGY AND SOLAR IRRADIANCE MONITORING ON SOHO

CLAUS FRÖHLICH[1], BO N. ANDERSEN[2], THIERRY APPOURCHAUX[3], GABRIELLE BERTHOMIEU[4], DOMINIQUE A. CROMMELYNCK[5], VICENTE DOMINGO[3], ALAIN FICHOT[5], WOLFGANG FINSTERLE[1], MARIA F. GÓMEZ[6], DOUGLAS GOUGH[7,8], ANTONIO JIMÉNEZ[6], TORBEN LEIFSEN[9], MARC LOMBAERTS[5], JUDIT M. PAP[10,11], JANINE PROVOST[4], TEODORO ROCA CORTÉS[6], JOSÉ ROMERO[1], HANSJÖRG ROTH[1], TAKASHI SEKII[7], UDO TELLJOHANN[3], THIERRY TOUTAIN[4] and CHRISTOPH WEHRLI[1]

[1]) Physikalisch-Meteorologisches Observatorium Davos
World Radiation Center, CH-7260 Davos Dorf
[2]) Norwegian Space Centre, N-0309 Oslo 3
[3]) Space Science Department, ESTEC, NL-2200 AG Noordwijk
[4]) Departement Cassini, URA CNRS 1362,
Observatoire de la Cote d'Azur, F-06304 Nice Cedex 4
[5]) Institut Royal Météorologique de Belgique, B-1180 Bruxelles
[6]) Instituto de Astrofísica de Canarias,
Universidad de La Laguna, E-38071 La Laguna, Tenerife
[7]) Institute of Astronomy, University of Cambridge,
Cambridge CB3 0HA, UK
[8]) Department of Applied Mathematics and Theoretical Physics,
University of Cambridge, Cambridge CB3 9EW, UK
[9]) Institute of Theoreretical Astrophysics, University of Oslo, N-0315 Oslo
[10]) Department of Physics and Astronomy, Division of Astronomy and Astrophysics
University of California, Los Angeles, CA90095-1562
[11]) Jet Propulsion Laboratory, California Institute of Technology,
Pasadena, CA 91109 USA

received 21 October 1996; revised ....

Abstract. First results from the VIRGO experiment (Variability of solar IRradiance and Gravity Oscillations) on the ESA/NASA Mission SOHO (Solar and Heliospheric Observatory) are reported . The observations started mid-January 1996 for the radiometers and sunphotometers and near the end of March for the luminosity oscillation imager. The performance of all the instruments is very good, and the time series of the first 4–6 months are evaluated in terms of solar irradiance variability, solar background noise characteristics and p mode oscillations. The solar irradiance is modulated by the passage of active regions across the disk, but not all of the modulation is straightforwardly explained in terms of sunspot flux blocking and facular enhancement. Helioseismic inversions of the observed p-mode frequencies are more-or-less in agreement with the latest standard solar models. The comparison of VIRGO results with earlier ones shows evidence that magnetic activity plays a significant role in the dynamics of the oscillations beyond its modulation of the resonant frequencies. Moreover, by comparing the amplitudes of different components of p-mode multiplets, each of which are influenced differently by spatial inhomogeneity, we have found that activity enhances excitation.

Key words: Helioseismology – Total Solar Irradiance – Spectral Solar Irradiance – p-Mode Excitation – SOHO Mission

1. Introduction

The VIRGO investigation (Variability of solar IRradiance and Gravity Oscillations) on SOHO (SOlar and Heliospheric Observatory) continues the research on solar irradiance variability and helioseismology. The aim of VIRGO is to determine the characteristics of pressure and internal gravity oscillations by observing irradiance and radiance variations, to measure the solar total and spectral irradiance and to quantify their variability over periods of days to the duration of the mission.

VIRGO contains two different active-cavity radiometers (DIARAD and PMO6-V) for monitoring the solar 'constant', two three-channel sunphotometers (SPM) for the measurement of the spectral irradiance at 402, 500 and 862 nm with a bandwidth of 5 nm, and a low-resolution imager (Luminosity Oscillation Imager, LOI) with 12 'scientific' and 4 guiding pixels, for measuring the radiance distribution over the solar disk at 500 nm. The instrumentation has been described in detail by Fröhlich *et al.* (1996). In addition, the observed in-flight performance and operational aspects of the irradiance observations are described by Fröhlich *et al.* (1997), and those of the LOI by Appourchaux *et al.* (1997).

SOHO was successfully launched on 2 December, 1995. VIRGO was switched on a few days later. The covers were kept closed for most of the time, but were released in order to outgas the experiment thoroughly during the following 7 weeks without having the optical surfaces exposed to the sun. On Christmas Eve all covers were opened for a short period of time in order to test the performance of the instruments in a 'first light' experiment. Real observations with the radiometers started mid-January, and observations with the sunphotometers at the end of January 1996. At that time it was realized that the LOI cover could not be opened. A concerted effort, as described by Appourchaux *et al.* (1997), was needed, and finally on 27 March the cover was successfully opened. The LOI has been operating continuously since the end of March 1996. The performance of all the instruments is very good.

The products of the VIRGO experiment are the following observational and derived data:

- continuous high-precision, high-stability and high-accuracy measurements of the solar total and spectral irradiance and spectral radiance and their variation;
- continuous measurements of the solar polar and equatorial diameter;
- frequencies, amplitudes and phases of oscillation modes in the frequency range of <0.1 μHz to 8 mHz.

The observational data products are time series which are corrected for all *a priori* known effects such as temperature, pointing, instrument–sun distance and relative velocity (for level 1), and inferred effects such as degradation (for level-2 data products). The present scientific evaluation is carried out on preliminary level-2 data, which may change in the future owing to improvements in the production of level-2 data from level-1 data. Such datasets from the first 4–6 months of operation are the basis for the results we present here. The following sections describe contributions to the study of total and spectral irradiance variability, namely the influence of active regions on irradiance variability and the characteristics of the solar background 'noise'. For helioseismology, frequencies and linewidths of the low-degree p modes ($l = 0 \ldots 7$) in the frequency range from 2150 to 3850 μHz ($n = 13 \ldots 27$) are presented, together with a preliminary interpretation from inversions. Furthermore, the temporal amplitude variation of p modes is examined.

2. Solar Irradiance Variability

2.1 Total and spectral solar irradiance and radiance measurements

Observations of the total solar irradiance are a continuation of previous measurements from satellites, which have been performed by several experiments since the end of 1978. For a discussion of these results and their relative behaviour see e.g. Fröhlich (1997). Fig. 1 shows the daily mean total solar irradiance data since 1980 (from Fröhlich, 1997 and references therein) supplemented by the VIRGO values until August 10, 1996.

The performance of the VIRGO radiometers and the procedures for the data evaluation are described by Fröhlich *et al.* (1997); in the following, the most important characteristics are summarized. The radiometers are operated in active mode, and have a basic sampling cadence of 3 minutes for the DIARAD and of 1 minute for the PMO6-V. Originally the latter was 2 minutes; the change is due to the fact that the PMO6-V shutters ceased to operate shortly after the start of the measurements. The PMO6-V radiometer is now operated quasi-continuously, with a reference value obtained every 8 hours by closing the cover (not the shutter) for about 6 minutes. This extends the accessible frequencies of variation into the p-mode range, thereby allowing p modes to be studied also with total irradiance data. The continuously exposed left DIARAD channel shows no measurable degradation up to August 1996. This conclusion was obtained from several comparisons with the right DIARAD channel which is operated about every 60th day for 30 minutes. In contrast, the operational PMO6-V radiometer degrades at a rate of ≈ 2.6 ppm/day relative to DIARAD. It is interesting to note that similar radiometers of both types (DIARAD and PMO6-V) on EURECA showed a degradation similar to that of the VIRGO PMO6-V,

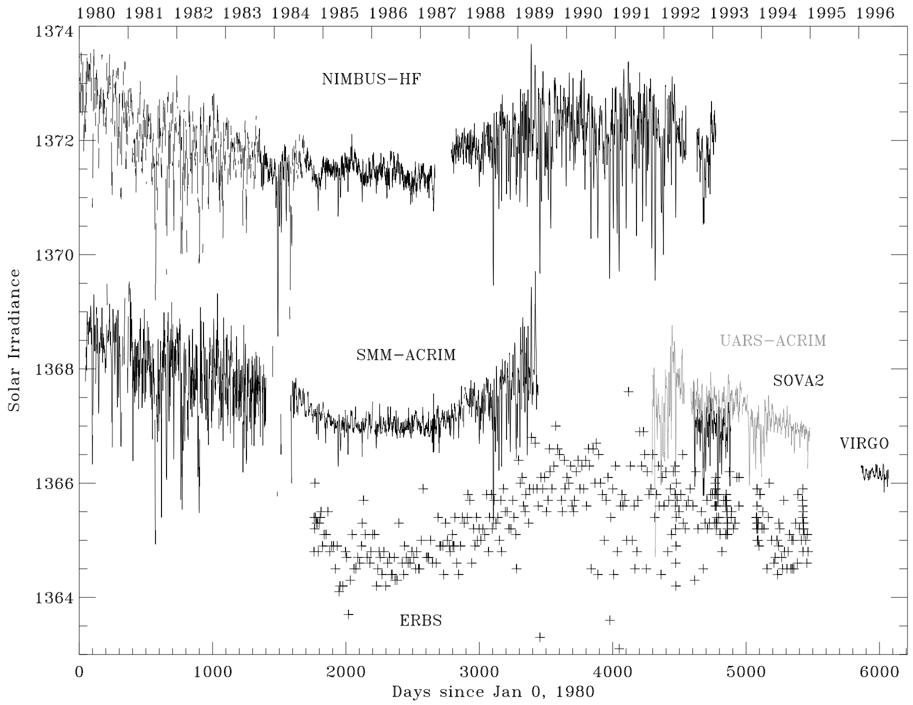

Fig. 1. Daily values of total solar irradiance since 1980 from Fröhlich (1997) supplemented by VIRGO data.

if referred to the same exposure times, whereas on SOHO the DIARAD photometer behaves quite differently. There are also some small differences in the time series of both radiometers which are not readily explained and which need investigation.

The absolute irradiance values are deduced from the radiometric characterization of each radiometer obtained before launch. In space the two radiometers differ by only 0.4 Wm^{-2}, namely 0.03%; this small difference is obviously fortuitous as the estimated absolute accuracy of each radiometer is $\approx$ 0.15%. The VIRGO solar irradiance values as shown in Figs. 1 & 2 are DIARAD values increased by 0.2 Wm^{-2} to account for the difference between both radiometers. The absolute values will be checked against measurements with similar radiometers on planned stratospheric balloon in spring 1997 and later with the experiment SOLCON onboard the NASA Hitchhiker program (Crommelynck *et al.* 1996), and complemented by a detailed study of the time series of simultaneous measurements of VIRGO and ACRIM-II on UARS.

The spectral irradiance data from the SPM are used to study the solar variability and solar oscillations; results from the former are presented in

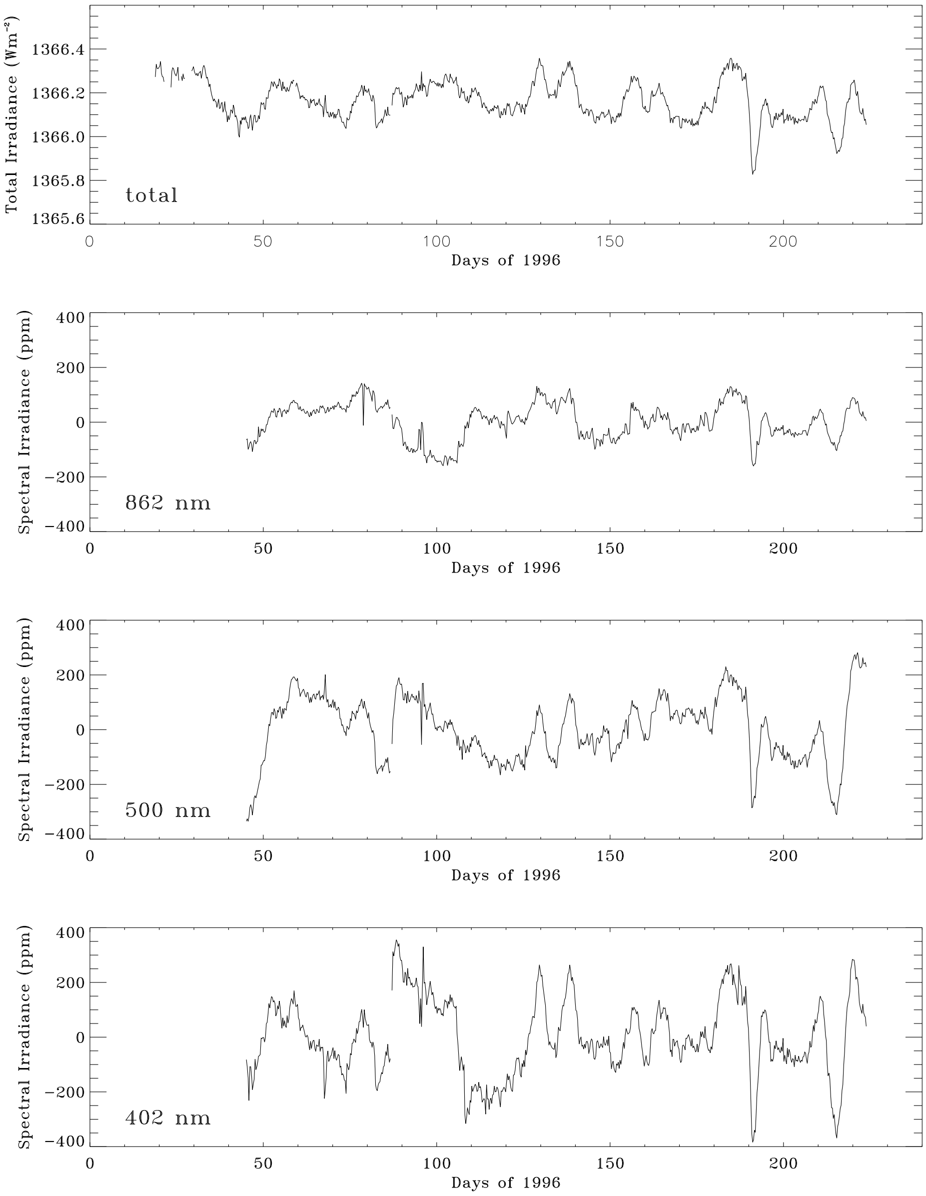

Fig. 2. 6-hours averages of total solar irradiance in Wm^{-2} and detrended spectral irradiance at 862nm, 500nm and 402 nm in ppm observed by VIRGO.

this section, those from the latter in Section 3.. The performance of the SPM and the procedures for the data evaluation are described by Fröhlich *et al.* (1997); here we summarize the most important characteristics. The sensitivity of the main instrument has slowly degraded with rates of about −52 ppm/day for the 862nm, −310 ppm/day for the 500nm and −650 ppm/day for the 402nm channel. These rates are determined assuming a constant solar irradiance over the period of evaluation. They are an order-of-magnitude lower than what was experienced by similar SPM instruments on EURECA or PHOBOS; more stable filters and strict cleanliness control during construction and in the spacecraft have indeed paid off. The spare instrument has been exposed only 4 times for 18-minute intervals, and shows no net trend; this is compatible with the observations of the total solar irradiance, and indicates that the assumption of constancy is reasonable. The detrended time series are shown in Fig. 2 together with the total solar irradiance.

During the 'first light' experiment all three irradiances were about 2.9% below the values of the spectrum of Neckel & Labs (1984). While this is still within the combined errors of the NBS-1973 spectral irradiance scale of the lamps used and the reference spectrum of Neckel & Labs (1984), the lower values of all channels hint at a systematic error during calibration. The absolute value will be checked during the stratospheric balloon flight planned for 1997 by comparing with a similar SPM calibrated before and after the flight, by means of the recently developed, very accurate radiometric method (Friedrich *et al.* 1996) instead of with standard lamps.

The variations seen in the time series of spectral and total irradiance are caused by a superposition of random and periodic phenomena. Variability caused by individual phenomena at the photosphere is modulated further by the solar rotation, leaving a very complicated mixture of temporal and spatial effects. Although the main objective of the LOI is the study of solar oscillations (Section 3.), its spatial resolution allows us to deconvolve the effects of different spatial and temporal influence of photospheric variations on the solar irradiance. The performance of the LOI and the procedures for the data evaluation are described by Appourchaux *et al.* (1997); in the following the most important characteristics are summarized. The signals from the 16 pixels are corrected to fluxes measured at 1 AU, using the orbital data to take into account the real shape of the pixels, the limb darkening at 500 nm, and the in-flight size of the solar image. In addition, for comparing the LOI integrated flux with the SPM, four conversion factors are derived for each type of pixel. These factors take into account the pixel shape, the limb darkening and the insensitive lanes between the pixels. Since the variation of these factors is slow, they are calculated only each day. Using the four SPM conversion factors we compared over the period of simultaneous measurements the LOI integrated flux with the one from the SPM green channel. The LOI sensitivity decreases much faster with time than the SPM 500 nm channel. At the beginning of the exposure it amounted to about 1000 ppm/day, decreasing to 500 ppm/day after 100 days. The stronger degradation is probably due partly to the fact that the LOI entrance filter sees more solar wind particles because of the rather large viewing angle of the filter to space, and is partly a result of having different coatings on the front surfaces. After correction by degradation, the LOI integrated flux compares quite well with the SPM, as shown by Appourchaux *et al.* (1997). Moreover, there is no indication of relative sensitivity changes between different pixels. Thus, the LOI is well suited to distinguish between spatial and temporal variability in the SPM and radiometer signals.

2.2 Solar noise

The continuous measurements allow us to produce for the first time alias-free power spectra of the variance of total and spectral irradiance over a wide range of frequencies corresponding to periods from 2 minutes to the duration of observation. This not only permits studies of the Sun with helioseismology, but also allows us to study the variability itself. In Fig. 3 the power density spectra of the total and spectral irradiance are shown. The most important features are:

- the p-mode signal stands above the solar background noise with a signal to noise at the peak of about 40:1;
- there is no visible excess in the solar noise in the p-mode region;
- in and above the p modes, the solar noise decreases with frequency as about ν^{-4}; this value depends weakly on the wavelength of the observations, the blue and green channels being the steepest;
- from 10 to 100 μHz the solar noise decreases with frequency as ν^{-2};
- from 100 to 800 μHz the solar noise spectrum is quite flat; this was not expected, and it is a very encouraging finding because this is the range where g modes are expected;
- a distinct hump in the power spectrum is seen at about 1.2 mHz in all spectra;
- fitting the spectra with function types proposed by Harvey (1985) gives time constants of the three regimes of the solar noise to be about 66, 480 and 40000 seconds; this indicates that there are no structures visible with time constants in the mesogranulation regime; the shortest time constant could possibly be attributed to network bright points;
- at low frequencies peaks exist corresponding to periods of about 27, 9 and 7 days which are related to activity features crossing the visible disk.

If one compares the total irradiance spectrum with the one deduced from orbital mean data of SMM-ACRIM in 1984/85 (Fröhlich *et al.* 1991) one notices that the power in the latter between about 40 μHz and the Nyquist frequency of 86 μHz is up to a factor of 3 higher than the one observed by the VIRGO radiometers. This an artifact from folding back high-frequency noise due to incomplete coverage during an orbit, and demonstrates that

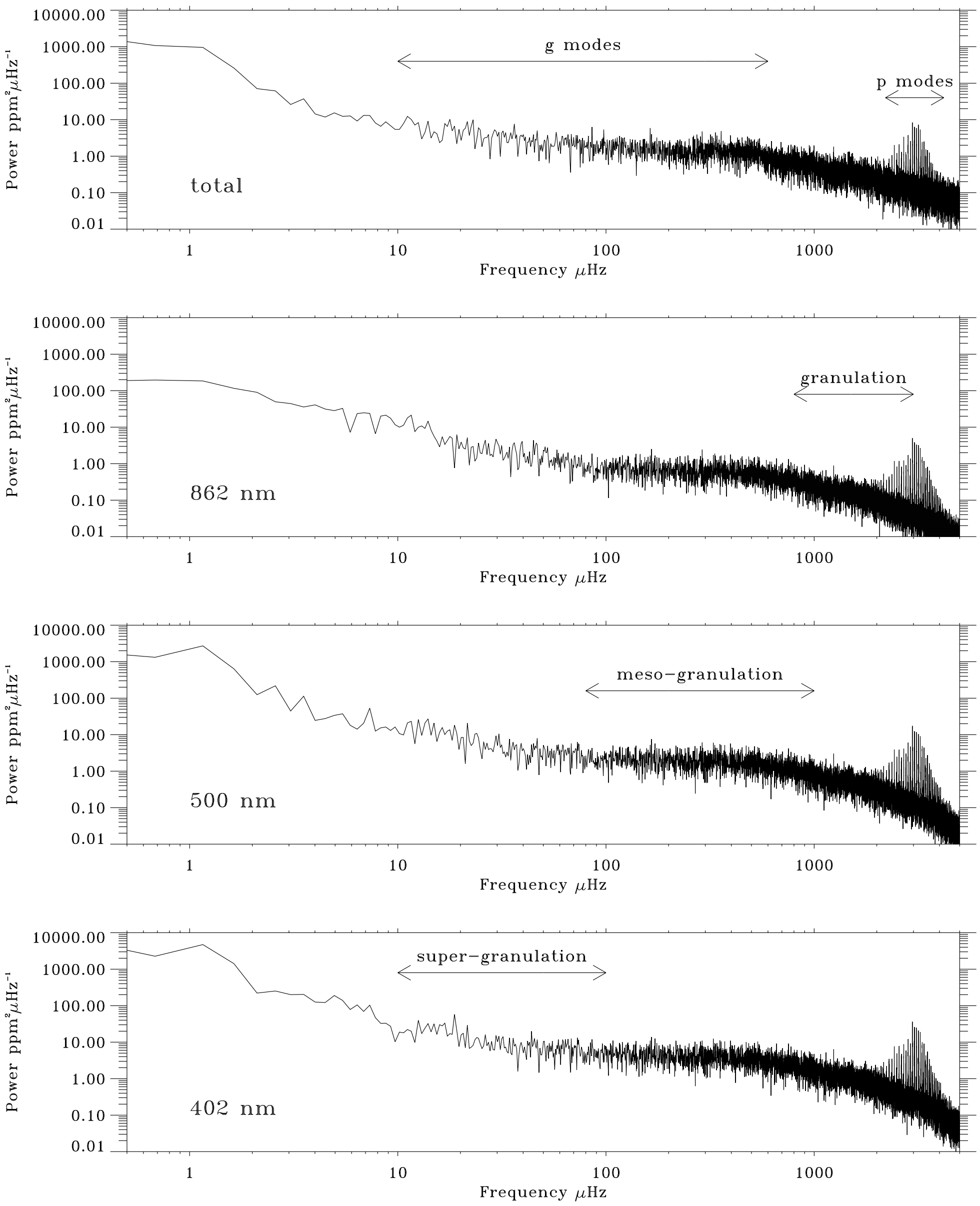

Fig. 3. Power spectra of total and spectral irradiance time series for the period from January, 28 until August, 10 1996.

continuous time series are a necessary prerequisite for unbiased power spectra.

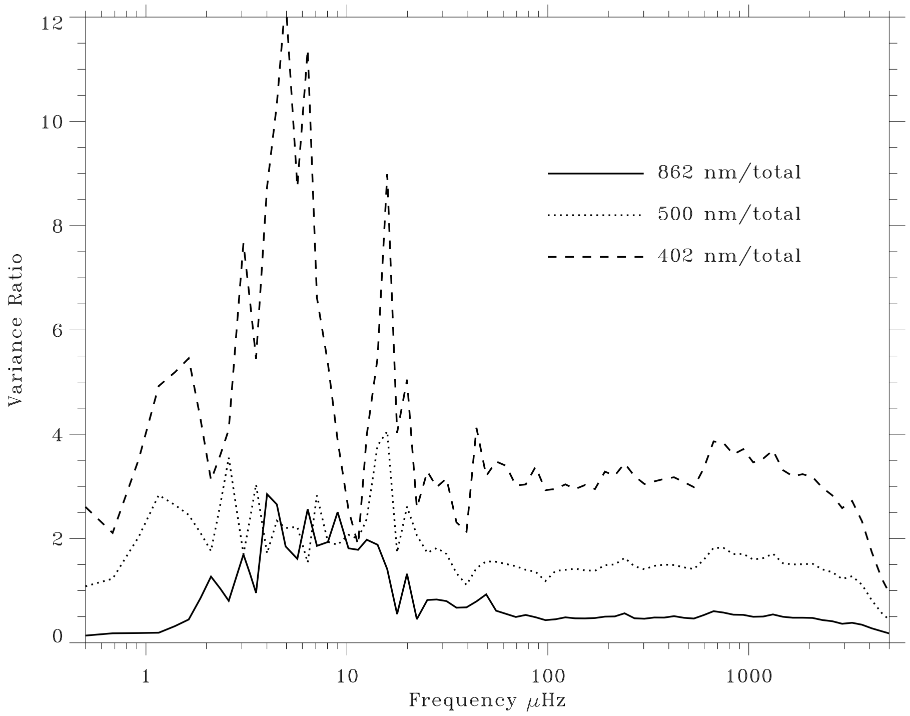

Fig. 4. Ratio of the power spectra from Fig. 3 of the spectral channels to the one of total irradiance.

Another new result is shown in Fig. 4 where the ratio of the variance of the different spectral channels to that of total irradiance is plotted. It shows a complicated dependence of these ratios upon frequency. In the frequency range of granulation and meso-granulation they are more or less constant, then they decrease towards lower frequencies with a broad minimum with about equal ratios for all colours at around 10 μHz, and then at even lower frequencies there is a broad hump at periods of a few days.

2.3 Influence of active regions

The time scales associated with the lifetime of magnetically active regions have revealed extremely interesting variations in total solar irradiance. Analyses based on former observations of total solar irradiance showed that the most striking events in the short-term irradiance changes are the sunspot-related temporary dips (Willson *et al.* , 1991). The fundamental question is whether the observed short-term changes are real luminosity changes or whether they represent a simple redistribution of the solar irradiance by sunspots and active regions faculae (Kuhn, 1996). To distinguish between these possibilities and to understand the underlying physical mechanisms of solar variability, it is important to study the spectral distribution of the variations observed in the entire solar flux. The VIRGO experiment provides the first high-precision observations of solar spectral irradiance at 402, 500, and 862 nm in parallel with the total solar irradiance observations. These observations permit the study of simultaneous temporal changes in the near-UV, visible, and infrared ranges, and to determine the spectral distribution of total solar irradiance variations, as is quite evident from Fig. 2. The most prominent passages of small active regions have their central meridian transit around days 120, 147, 182 and 202. Here we discuss the first one (occurrence of active region NOAA 7962 in early May 1996).

At the top of Fig. 5 we show magnetograms from Mt Wilson to illustrate the active region, and below we show time series of the total and spectral irradiance and of the four southern pixels of the LOI. The active region is causing significant changes in the spectral irradiance in the blue and green channels and the LOI, and much less in total irradiance and in the near IR. This particular active region appeared close to the limb in the southern part of the visible solar disk on 6 May (day 127) and contained a very small sunspot which vanished around 14 May. Very close to this region, a smaller active region without sunspots was also visible.

The LOI east pixel intensity value started to rise around 6 May with the appearance of the faculae in the active region rotating onto the east limb of the solar disk with a primary peak three days later. In parallel with the LOI east pixel intensity increase, both total solar and spectral irradiance in all the 3 wavelengths started to increase. When referring the intensities to the level of the quiet sun before and after the passage, the largest of the increases in irradiance within a 4-day of period was measured in the blue channel: it was about 300 ppm, and is to be compared about 200 ppm for the green channel and about 100 ppm in both the red channel and the total irradiance. It is interesting to note that at the meridian transit only the blue and green irradiances reached the quiet sun level, whereas the red channel and the total irradiance decreased by only about 40% and 60% of the total increase respectively. The photometric deficit of the spot group as determined by the San Fernando Observatory was around 50 ppm (Solar-Geophysical Data, 1996) at the maximum sunspot influence (around May 12–13). Taking the wavelength dependence of the spot contrast into account one would expect 45, 65 and 75 ppm for red, green and blue channels respectively. This accounts for only about half of the observed decrease in total irradiance by the sunspot darkening. The other half must be due to the facular contribution which is smaller at disk center. Photometric observations of faculae show a limb brightening and the facular contrast at the disk centre is close to zero or is even negative. The behaviour close to the limb can account for the strong peak of the irradiance at central meridian distances of about $\pm 60°$. The fact that only a partial decrease at the centre is observed

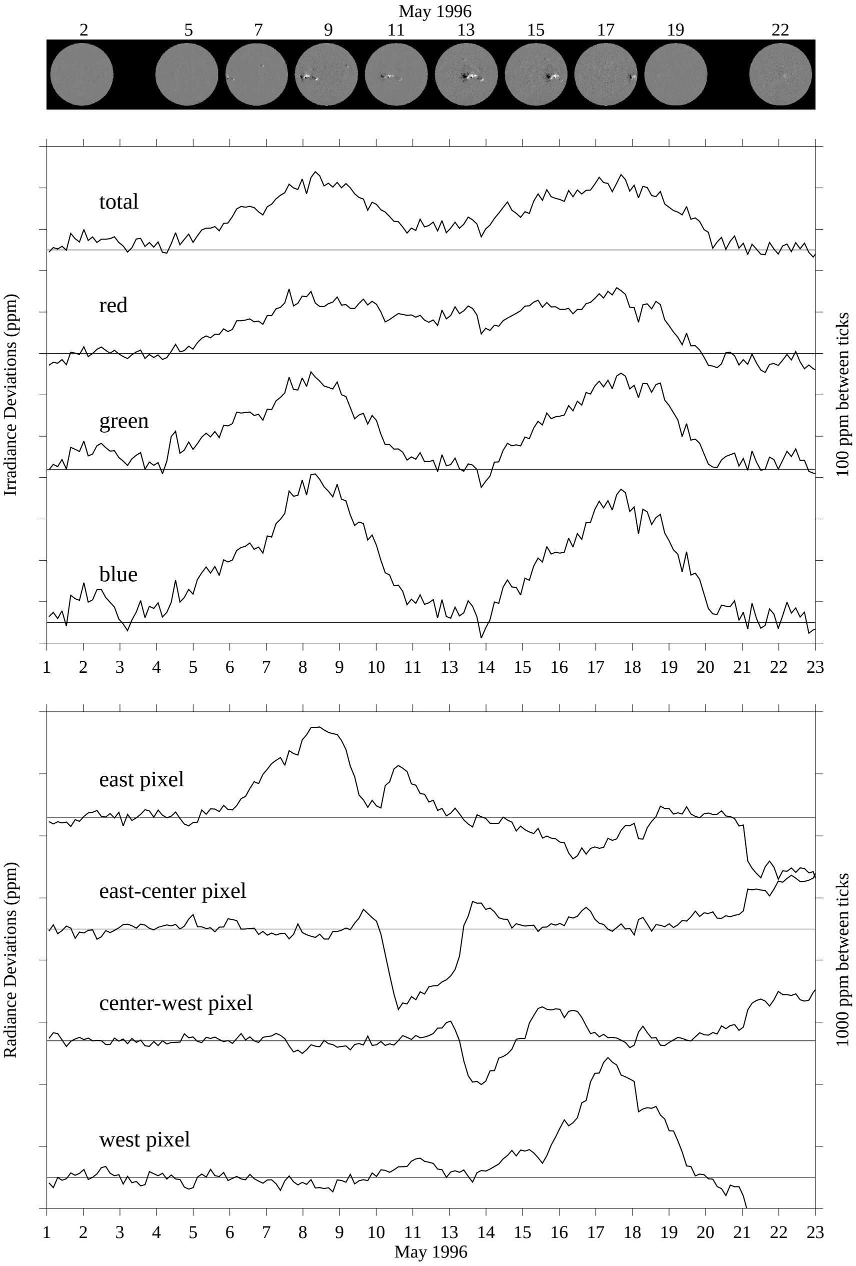

Fig. 5. Passage of the active region NOAA 7962 in May 1996 shown by the Mt Wilson magnetograms in the Fe I line (top panel, black and white correspond to ± 5 Gauss), the time series of total and spectral irradiance (middle panel) and of the four LOI pixels south of the equator (bottom panel).

indicates that the faculae are still seen in the spectral and total irradiance, or that the faculae extend over a much larger area than the magnetogram suggests. Moreover, the centre-to-limb increase depends strongly on wavelength, and must be substantially smaller in the red and total irradiance than in the green and blue.

The LOI radiance values confirm this general behaviour. The east pixel shows mainly the increase due to faculae; on the crossover to the next pixel the radiance first increases due the faculae in front of the active region and then it suddenly decreases due to the dark spot. The effect of the 65 ppm in the green sun-as-a-star signal is greater by a factor of about 12, owing to the smaller area of the pixel, yielding a decrease down to about -1100 ppm; then the spot slowly vanishes, indicated by the steady increase of the radiance. The change over to the next pixel shows again an increase and then the decrease due to the now smaller spot. At the central crossover there is still an increase, indicating that indeed the faculae are still bright close to the centre. This whole sequence shows very interesting details of how active regions influence the irradiance. Yet more detailed studies will definitively reveal clues for the understanding of irradiance and radiance variability.

3. Solar Oscillations

The analysis is based on the power spectra calculated from the time series of the SPM channels and the 12 LOI pixels. The time series are detrended by piecewise fits of quadratic polynomials for the SPM and with a curve obtained by triangular smoothing with a full width of one day for the LOI. The power spectra are calculated from the Fourier transform of apodized time series then by squaring the complex amplitude. As an example the p-mode spectra of the total, red, green and blue irradiance are shown in Fig. 6. Note the high signal-to-noise ratio for the SPM channels and the lower one for the total irradiance. This is due to the sampling duty cycle of only 31% for the PMO6-V observations compared to the SPM with 94%. The ratios of the increasing amplitudes observed in the red, total, green and blue are ≈0.4:0.5:0.7:1.0. Another clearly seen feature is the relative increase of the amplitudes of the higher degree modes from red to blue as shown by the ratio of the $l = 2$ to the $l = 0$ (e.g. around 3030 μHz) or the $l = 3$ to the $l = 1$ (e.g. around 2950 μHz), albeit less obvious due to the low visibility of the $l = 3$ mode. This is due to the increasing center-to-limb variation towards the blue which weights the central part of the disk more and more and increases the visibility of the higher degrees relative to lower ones.

3.1 Data reduction

From the SPM spectra the p-mode parameters are derived by fitting Lorentzians using a maximum-likelihood method as described in Toutain and Fröh-

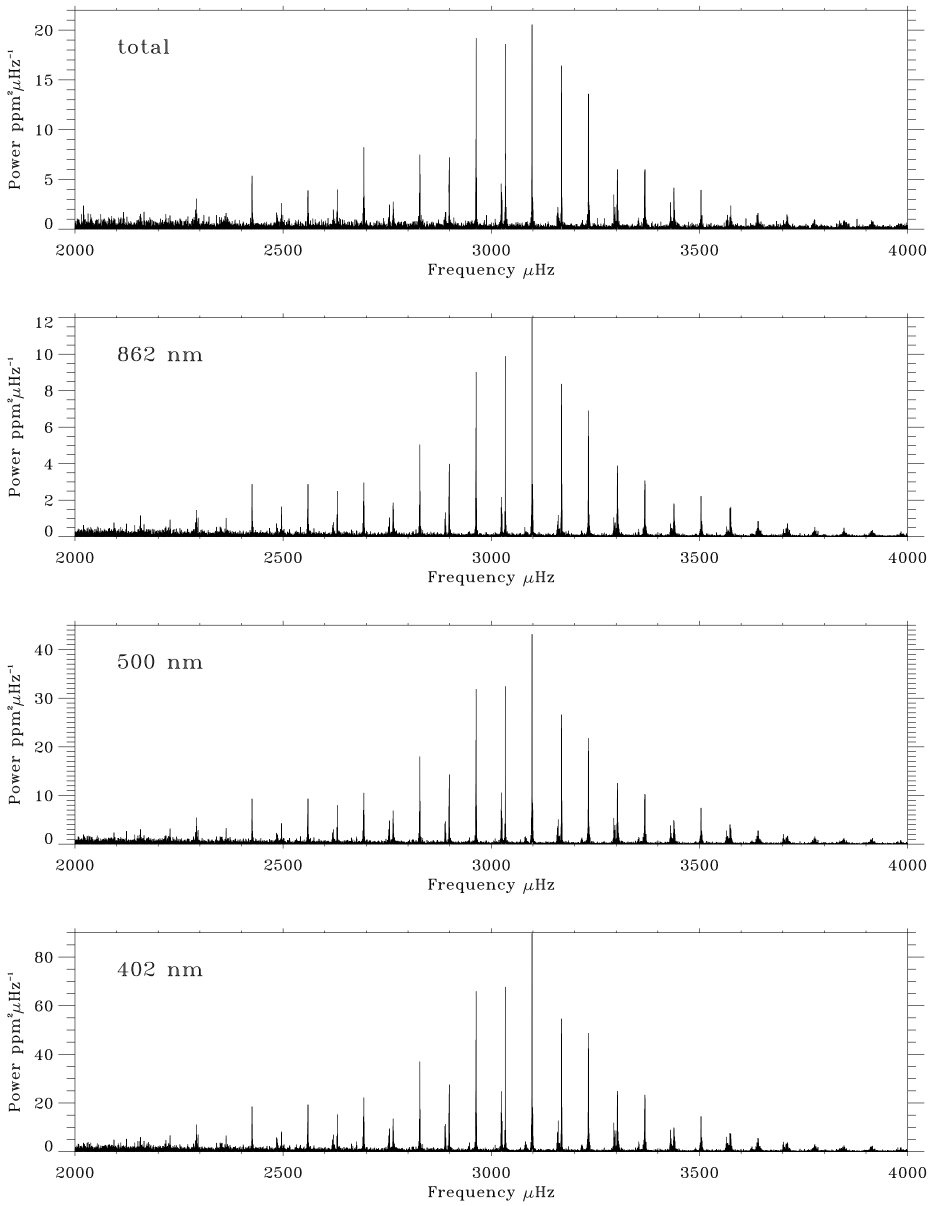

Fig. 6. p-mode spectra from about 200 days of observation of the total, red, green and blue irradiance.

lich (1992). The only difference is that the mode amplitudes in a given (l, m) multiplet are no longer constrained to be the same. For the LOI a given (m, ν) diagram is fitted simultaneously using a maximum-likelihood method

TABLE I
Comparison of the $l = 0$ frequencies determined from the LOI and the three SPM channels.

n	LOI	RED	GREEN	BLUE
15	2228.34 $\pm$0.086	2228.499 $\pm$0.097	2228.434 $\pm$0.118	2228.440 $\pm$0.113
16	2362.96 $\pm$0.120	2363.108 $\pm$0.094	2363.107 $\pm$0.095	2363.106 $\pm$0.095
17	2496.14 $\pm$0.088	2496.233 $\pm$0.083	2496.219 $\pm$0.088	2496.238 $\pm$0.085
18	2630.03 $\pm$0.151	2630.014 $\pm$0.088	2629.948 $\pm$0.089	2629.996 $\pm$0.094
19	2764.43 $\pm$0.156	2764.367 $\pm$0.117	2764.326 $\pm$0.115	2764.311 $\pm$0.119
20	2898.95 $\pm$0.097	2899.028 $\pm$0.082	2898.983 $\pm$0.087	2898.970 $\pm$0.078
21	3033.75 $\pm$0.085	3033.683 $\pm$0.060	3033.662 $\pm$0.058	3033.668 $\pm$0.058
22	3168.67 $\pm$0.085	3168.610 $\pm$0.072	3168.559 $\pm$0.066	3168.556 $\pm$0.067
23	3303.21 $\pm$0.114	3303.232 $\pm$0.094	3303.205 $\pm$0.091	3303.228 $\pm$0.092
24	3438.95 $\pm$0.160	3438.863 $\pm$0.126	3438.854 $\pm$0.132	3438.860 $\pm$0.133
25	3574.62 $\pm$0.291	3574.855 $\pm$0.219	3574.630 $\pm$0.225	3574.719 $\pm$0.227

as described in Appourchaux *et al.* (1995). Moreover, the crosstalk between the $2l+1$ components of a multiplet as well as the aliases from higher-degree modes are appropriately taken into account (Appourchaux *et al.* , 1997).

3.2 Frequencies of p modes

The most important parameters of the p-mode characteristics are the frequencies. Four such sets are available in VIRGO. As the degeneracy splitting is not resolved in the low-degree modes determined from global observations of the sun the frequencies of the $l = 1, 2$ from the SPM spectra can be biased. The frequencies of the uninfluenced $l = 0$ modes determined from the SPM channels are in good agreement among themselves and with the ones determined from the LOI as shown in Table I. There might be, however, a systematic decrease of the frequencies from the red to the blue. This effect cannot be the influence of excitation noise as the same realizations are observed in all three colours. It could be due to an effect in the solar atmosphere changing the assymetry of the line profile with height which may then be interpreted as a frequency shift because it is analysed assuming a symmetric profile.

In order to have an internally consistent data set we present as VIRGO first-result frequencies those determined from LOI. These frequencies are listed in Table II. They can be compared to those determined by the IPHIR experiment (Toutain & Fröhlich, 1992) during the second half of 1988. Fig. 7 shows the result of this comparison, and it is interesting to note that the fre-

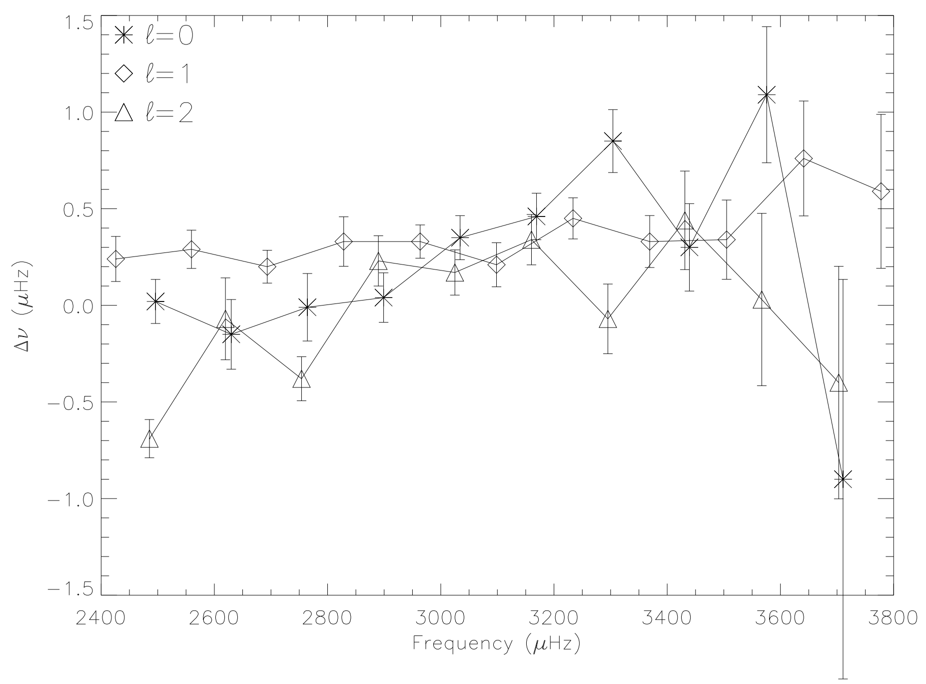

Fig. 7. Comparison of the VIRGO frequencies with the ones determined by IPHIR.

quencies of the $l = 1$ modes are systematically higher, with a slight increase towards higher frequencies which could well be due to differences in solar activity.

3.3 Linewidths and Amplitudes

Linewidths are determined from the same fitting procedure from both the SPM green channel and the LOI. The results are shown in Fig. 8. Note the pronounced dip around the peak of the 5-minute oscillations. This dip is a resonance effect with convection which decreases the damping of the modes, and was predicted by Gough (1980; cf Balmforth, 1992). It is interesting that the IPHIR data did not show this dip, which is suggesting that the resonance effect may be decreased by increasing solar activity.

Detailed studies of the time variation of mode amplitudes for solar p modes are essential for understanding both the excitation mechanisms and the response of the solar surface to the perturbations caused by the modes. In this context it is crucial to understand that the properties of the solar surface acts as a filter between the oscillations and the observer. These studies require continuous data sets.

Wavelet analysis is an appropriate tool for studying time-dependent phe-

TABLE II
List of frequencies of solar p modes determined from VIRGO.

order	l=0	l=1	l=2	l=3
13	-	-	-	2137.79± 0.07
14	-	-	2217.63 ±0.08	2273.47±0.06
15	2228.34±0.09	2292.17 ±0.05	2352.29 ±0.07	2407.73±0.09
16	2362.96±0.12	2425.68 ±0.10	2486.05 ±0.07	2541.70±0.06
17	2496.14±0.09	2559.29 ±0.07	2619.69 ±0.08	2676.23±0.05
18	2630.03±0.15	2693.32 ±0.07	2754.44 ±0.07	2811.49±0.06
19	2764.43±0.16	2828.19 ±0.08	2889.59±0.05	2946.97±0.04
20	2898.95±0.10	2963.32 ±0.08	3024.75±0.04	3082.31±0.04
21	3033.75±0.09	3098.16 ±0.11	3159.83±0.07	3217.74±0.05
22	3168.67±0.09	3233.21 ±0.04	3295.25 ±0.06	3353.58±0.07
23	3303.21±0.12	3368.64±0.11	3430.76±0.11	3489.65±0.08
24	3438.95±0.16	3504.39 ±0.17	3567.02±0.15	3626.35±0.12
25	3574.62±0.29	3640.35 ±0.24	3703.41±0.22	3763.01±0.18
26	3711.45±0.98	3777.07 ±0.18	3840.84±0.31	-
27	3847.28±1.57	-	-	-

order	l=4	l=5	l=6	l=7
13	2188.43 ±0.35	2235.42 ±0.02	2280.08 ±0.07	2322.40 ±0.09
14	2324.31±0.05	2371.23±0.07	2415.59 ±0.06	2458.25 ±0.07
15	2458.53±0.05	2506.00±0.06	2551.12±0.05	2594.27±0.06
16	2593.16±0.08	2641.25±0.04	2687.08±0.05	2731.08 ±0.09
17	2728.51±0.09	2777.24±0.07	2823.81±0.05	2868.40±0.05
18	2864.28 ±0.09	2913.51±0.04	2960.62±0.04	3005.54±0.04
19	3000.13±0.05	3049.84±0.05	3097.09 ±0.05	3142.77 ±0.04
20	3135.96±0.05	3186.26±0.05	3234.17 ±0.06	3279.76 ±0.05
21	3271.74 ±0.06	3322.67±0.10	3370.91 ±0.11	3417.35 ±0.07
22	3408.14±0.09	3459.74±0.12	3508.80 ±0.12	3554.93±0.15
23	3544.67±0.10	3596.35±0.17	3646.05 ±0.14	-
24	3682.25 ±0.16	3734.72±0.17	-	-

nomena. With an optimal selection of parameters this method also provides a better combined frequency and time resolution than is provided by conventional Fourier analysis. These methods have previously been successfully used on IPHIR data (Baudin *et al.* 1994, Leifsen *et al.* 1995). The amplitudes of the p modes from the SPM blue channel and the LOI have been studied with this method. The results from the LOI data on the $l = 1$ indi-

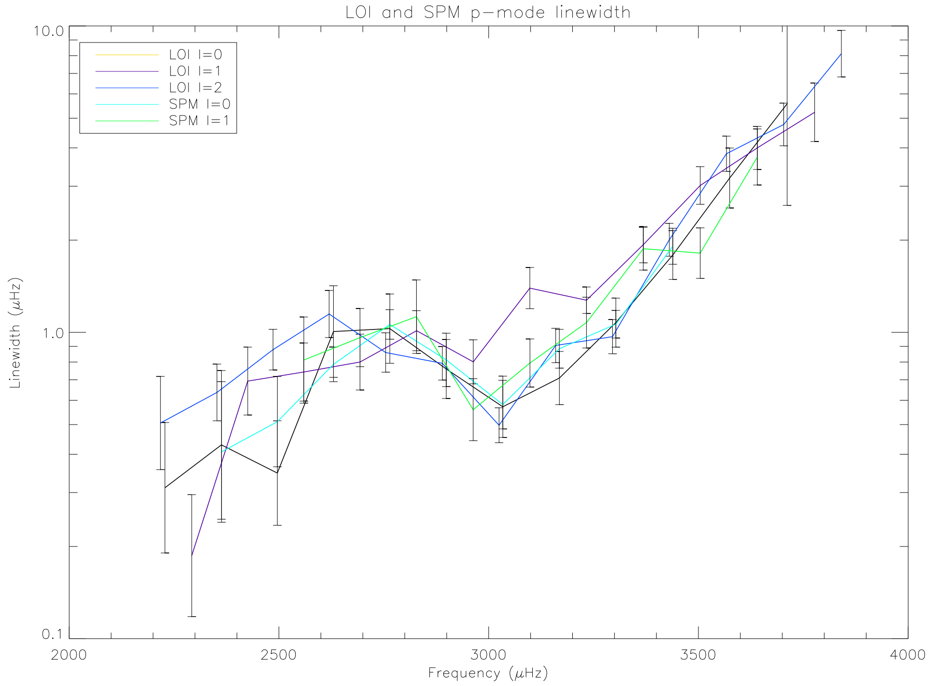

Fig. 8. Linewidth determined from the SPM green channel and LOI for $l = 0 \ldots 2$.

cate no correlation between the different rotationally split components of each radial order. This is to be expected from our view that the oscillations are excited randomly by the turbulence in the upper boundary layer of the convection zone, despite the fact that each individual excitation event applies equal impulses to eastward and westward propagating modes with like values of l and $|m|$. The results with high frequency resolution for the $l = 0, n = 16 - 26$ modes from the SPM blue channel are shown in Fig. 9. From the data we see no clear and consistent correlation of the excitation of the different modes. This too is as we expect (Chang, 1995). A prominent phenomenon is the clear variation of the central frequency position of the modes. Complicated structures with shifts and splittings of the modes are clearly seen. This is a result of phase wandering due to the excitation, and is manifest as a power variation in different regions of the mean Lorentzian profile of the modes. It shows the danger in fitting Lorentzians to the power spectra of modes obtained from short time strings of data. Such a fitting will give spurious frequency shifts. The required length of the time series to achieve a reasonable accuracy of the Lorentzian fitting may be so long that solar cycle variations could be masked.

The time dependence of the amplitude variation of the different modes

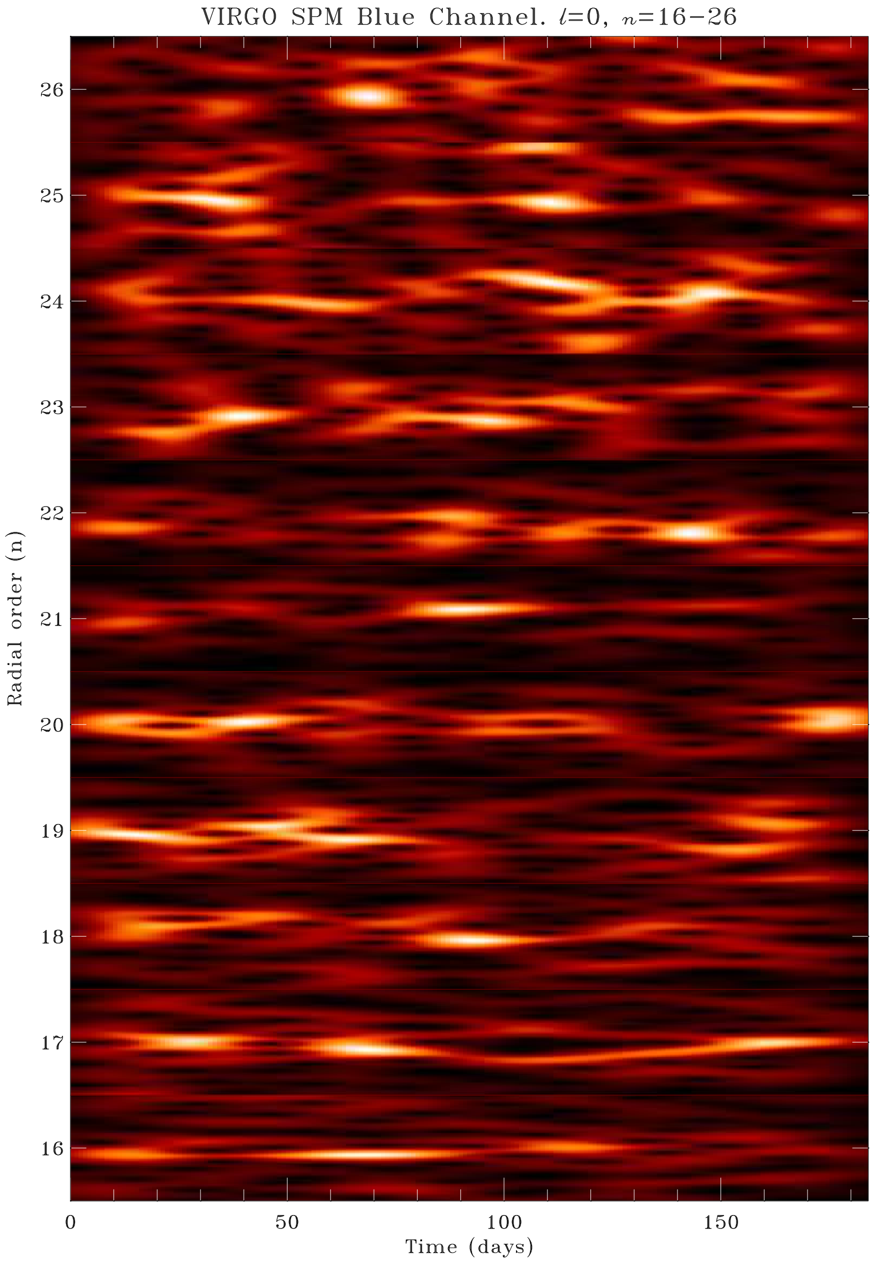

Fig. 9. Wavelet analysis of $l = 0, n = 16 \ldots 26$ from the SPM blue channel. The time axis starts on the January 29 1996. The frequency coverage for each radial order is 4 μHz.

have been studied by calculating the power spectra. For this, wavelet parameters giving a time resolution of about 10 hours was used. The possible effect of interference from the nearby $l = 2$ modes has been filtered out. The results are given in the upper panel of Fig. 10. The dominant peak is seen at approximately the position of the solar rotation and should be compared with the lower panel showing the periodicities in the irradiance signal. Within the current resolution some of the minor peaks are also common. The periodicities are also seen in the power spectra of the individual modes, but there the amplitudes of the different peaks vary strongly between the modes. From these results one cannot infer a latitudinal variation of the excitation. With current understanding of these mechanisms this would not create a discernible signal in the modulation. The explanation of the modulation stems from the variation of the solar surface structure, i.e. with active regions, which modulate what we observe. The response of the surface to the perturbations of the oscillations is different in active and quiet regions of the sun. Further observations are needed to see whether the periodicities in the amplitudes correspond to the mean solar rotation or to the rotation of the active regions.

Another interesting property of the oscillations concerns the relative amplitudes of the components of the multiplets. Although the datasets are perhaps not yet long enough to secure reliable statistics, there does appear to be a systematic variation in the power, as is illustrated in Fig. 11 Such a distribution is not inconsistent with preferential excitation of the oscillations in regions of enhanced activity. In particular, if we adopt a latitudinal variation of the excitation rate that has maxima at midlatitudes, we can account for the general trends in the observed amplitudes if the maximum excess rate of energy input into oscillations is about 50% of the uniform background. The best fit to the data of a smooth symmetric function with single maxima in each hemisphere has the maxima at about $\pm 40°$ latitude, which is similar to though somewhat greater than the mean latitudes of the sunspot belts early in the cycle. Nevertheless, the broad agreement does suggest that magnetic activity plays a role in exciting the oscillations, in addition to modifying their frequencies (cf Kuhn and Libbrecht 1991). The difference between the locations of the maxima in the excitation function that we have deduced and the locations of the sunspots could perhaps be a result of inadequate statistics, or it could perhaps be an artifact of having misjudged the instrumental sensitivity to different modes by ignoring the magnetic perturbation to the eigenfunctions which causes the apparent decrease in power which Brown (1991) has observed to occur in active regions. Alternatively, it could simply be that the regions of enhanced excitation extend beyond the observed regions of activity, as we were led to suspect from the variations in the radiance measurements discussed in section 3.2.

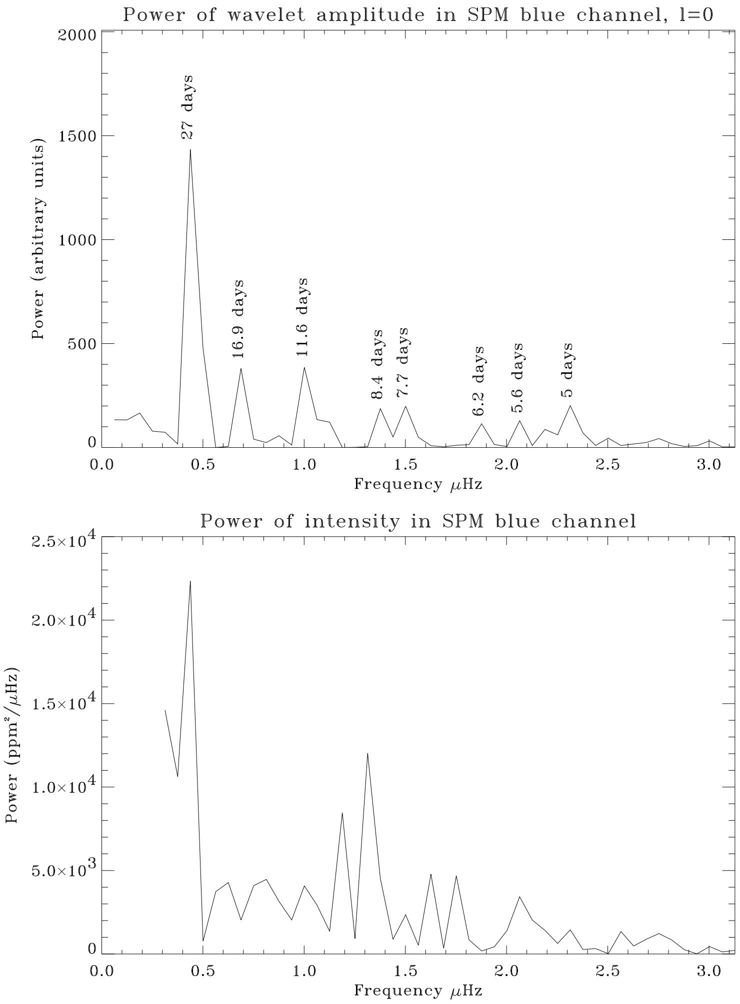

Fig. 10. Power spectrum of the average amplitude variation for the modes of Fig. 8 in the very low frequency range (upper panel). The most prominent peaks are labelled with the corresponding period in days. For comparison the power spectrum of the SPM blue channel is shown in the lower panel.

3.4 Inversions of the VIRGO frequencies

P-mode frequencies from Table II have been inverted to investigate the structure of the solar core. A total of 92 modes with $0 \leq l \leq 7$ were used in the frequency range 2.1mHz$\lesssim \nu \lesssim$3.8mHz. The mode with the shallowest inner turning point penetrates to $r/R_\odot \simeq 0.3$, and our investigation concentrates

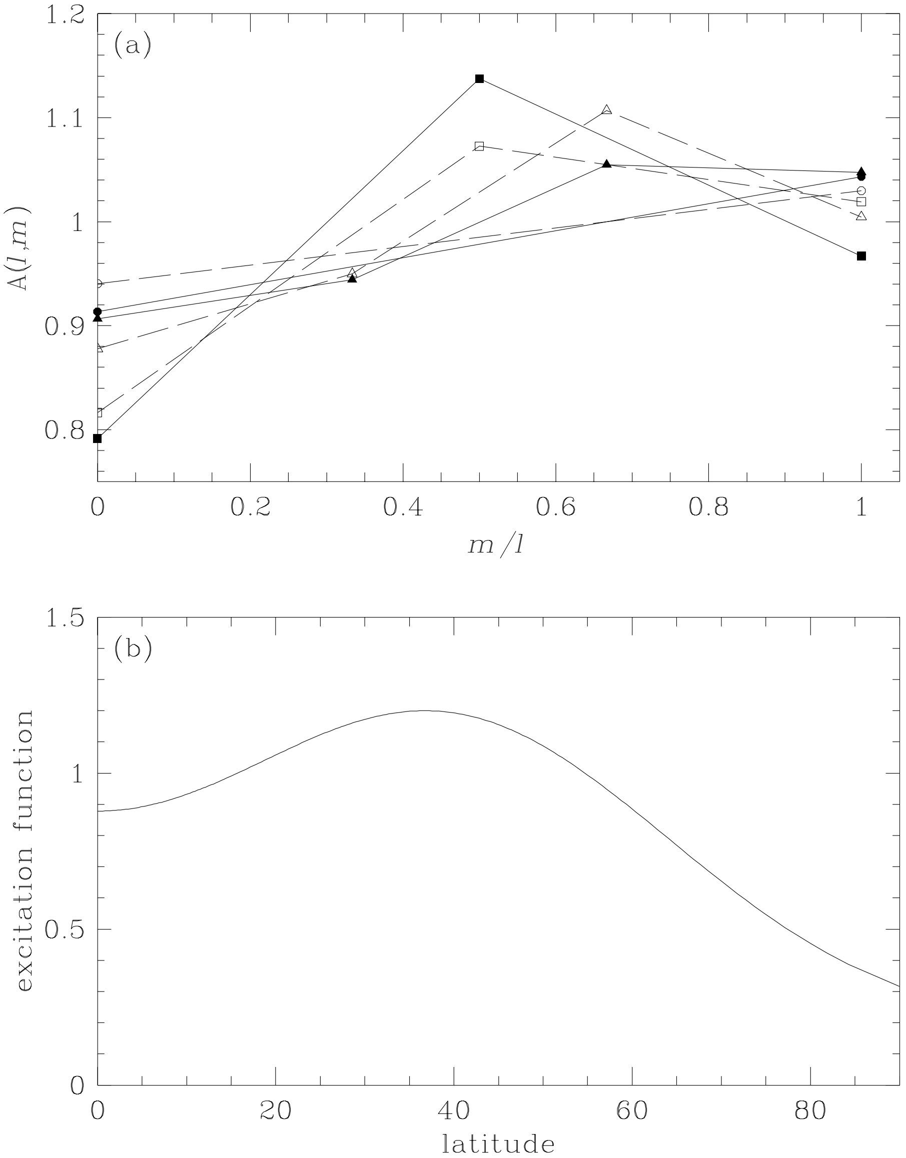

Fig. 11. (a) Mean relative amplitudes of the components of dipole (circles), quadrupole (squares) and octupole (triangles) multiplets, plotted against $|m|/l$. The amplitudes of each multiplet are normalized such that the mean power per mode is unity. Filled symbols joined by continuous lines are derived from observations by LOI; the corresponding open symbols joined by dashed lines are theoretical values computed assuming the latitudinal variation of energy input illustrated in (b).

on the layers below these depths, since outside these regions the datasets do not provide much information about the solar structure.

The standard strategy of linearization was adopted (e.g., Gough 1996): we use a theoretical model of the sun as a reference, and then consider the difference between the sun and the model. We attempt to determine how the sun differs from the reference model by considering the difference between the observed frequencies and those of the reference model. The relative frequency difference is equated to a linear functional of the difference in structures:

$$\frac{\delta\nu_i}{\nu_i} \equiv \frac{\nu_{\mathrm{obs},i} - \nu_i}{\nu_i} = \int \left[K^i_{u,\gamma_1}(r) \frac{\delta u}{u} + K^i_{\gamma_1,u}(r) \frac{\delta\gamma_1}{\gamma_1} \right] dr + \frac{F(\nu_i)}{I_i} , \tag{1}$$

where ν_i and $\nu_{\mathrm{obs},i}$ are respectively the frequencies of the model and the observed frequencies of the mode i. and K^i_{u,γ_1} and $K^i_{\gamma_1,u}$ are the kernels for the squared isothermal sound speed u and the adiabatic exponent γ_1, which are our choice of inversion variables. The two functions δu and $\delta\gamma_1$ are the differences between the values of u and and the ones of γ_1 in the sun and in the model. We present below inversions for δu. The term $F(\nu_i)/I_i$, where $F(\nu_i)$ is an unknown function of frequency (which we represent as an expansion in terms of Legendre polynomials) and I_i is the mode inertia (normalization is such that the vertical component of displacement eigenfunction is unity at the surface), is added to represent all the uncertainties that arise from our lack of knowledge of the subsurface layers (for detailed discussion see Gough 1995).

To carry out the inversions we used optimally localized averaging (e.g., Gough 1996; also Däppen *et al.* 1991); to estimate δu at radius r_0, we construct a linear combination of the relative differences,

$$\sum c_i(r_0) \frac{\delta\nu_i}{\nu_i} = \int \left(\sum c_i K^i_{u,\gamma_1} \right) \tfrac{\delta u}{u} dr + \int \left(\sum c_i K^i_{\gamma_1,u} \right) \tfrac{\delta\gamma_1}{\gamma_1} dr + \sum c_i \tfrac{F(\nu_i)}{I_i} \tag{2}$$

in such a way that it provides an estimate of a localized average of δu in the vicinity of $r = r_0$. Specifically, we choose the coefficients c_i that minimize

$$S \equiv \int K_{u,\gamma_1}(r, r_0)^2 (r - r_0)^2 dr + \alpha \int K_{\gamma_1,u}(r, r_0)^2 dr + \beta \sum_i c_i^2 \sigma_i^2 \tag{3}$$

subject to

$$\int K_{u,\gamma_1} dr = 1 \tag{4}$$

and

$$\sum_i c_i \frac{P_\lambda(\nu_i)}{I_i} = 0 \quad , \lambda = 0, \ldots, \lambda_{\max} , \tag{5}$$

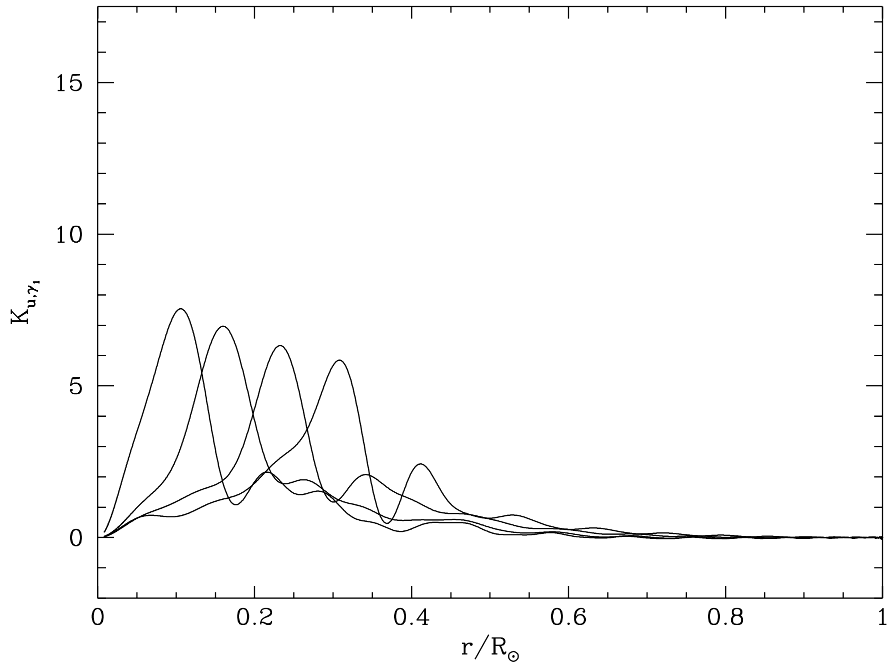

Fig. 12. Averaging kernels for squared isothermal sound speed u obtained from 92 LOI frequencies.

where

$$K_{u,\gamma_1}(r, r_0) \equiv \sum_i c_i K^i_{u,\gamma_1}(r) \ , \tag{6}$$

$$K_{\gamma_1,u}(r, r_0) \equiv \sum_i c_i K^i_{\gamma_1,u}(r) \tag{7}$$

are the averaging kernel for u and the kernel determining the contamination of the inference by $\delta\gamma_1$, and $P_\lambda(\nu_i)$ is a Legendre polynomial.

The first term in S encourages localization of the averaging kernel, which has unit modulus imposed by the first constraint; the second suppresses the amplitude of the contaminating kernel, and the third suppresses error magnification. Thus the parameters α and β are used to balance the weights between resolution, contamination from $\delta\gamma_1$ and error. The purpose of the second set of the constraints is to eliminate the contribution from the unknown surface layers, with a resolution determined by the value of $\lambda_{\max}$ in the Legendre decomposition of $F(\nu_i)$.

A selection of the averaging kernels we have obtained is shown in Fig. 12. Owing to the small number of modes, the degree of localization is not very good. To obtain better localization, it is essential to supplement the

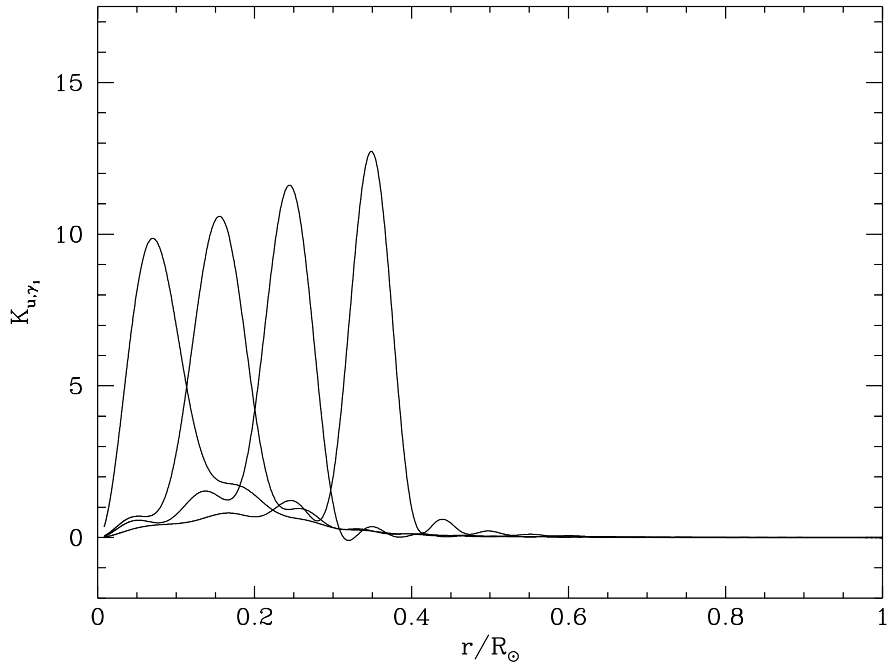

Fig. 13. Averaging kernels for squared isothermal sound speed u obtained from 1105 combined LOI+LOWL frequencies.

dataset with higher-degree modes. We used the LOWL dataset (Tomczyk *et al.* 1996) for this purpose. From the LOWL 2-year average dataset, 1013 modes with $l \geq 8$ in the frequency range 1.5mHz $\leq \nu \leq$ 3.5mHz were chosen and added to 92 LOI frequencies. The improved averaging kernels obtained from the combined dataset are shown in Fig. 13, which illustrates the importance of having higher-degree modes. Fig. 14 shows the result of the inversion, together with a result of a second inversion, where we excluded a single mode ($l = 0, n = 15$) because a problem with that mode was recognized during the analysis. We note how sensitive our inference of the deepest part of the sun can be to just a single mode. We also add a further word of caution, because there seem to be systematic differences between the LOWL and LOI frequencies for $l < 8$, which may come about from the different intervals of observation coupled with a systematic difference between the outcome of Lorentz fitting to velocity and radiance data or similar to the difference between the colours from an atmospheric effect. It is therefore incumbent upon us to carry out the frequency analysis with the greatest care before any definitive conclusion be drawn. From the current results alone there is no compelling evidence that the sun is substantially

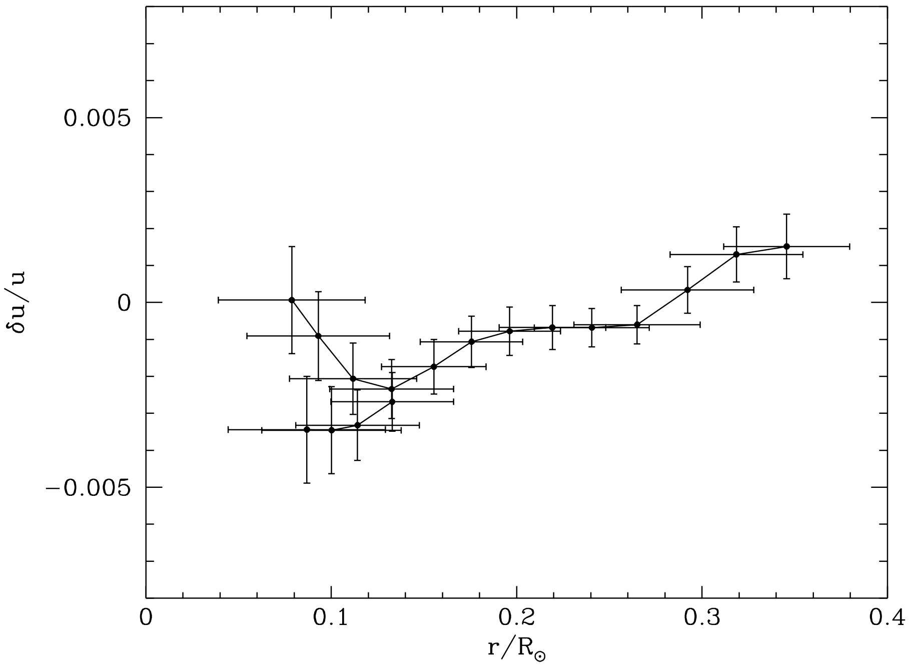

Fig. 14. The relative difference in the squared isothermal sound speed between the sun and the reference model, inferred from the LOI+LOWL frequencies. The lower curve represented by 4 points was obtained by excluding $l = 0, n = 15$ from the inversion; at greater values of $r/R_\odot$ the removal of the datum hardly influences the inversions.

different from the reference model.

4. Conclusions

All instruments within the VIRGO package work very well, and interesting new results have been gathered from our preliminary investigation of the first 4–6 months of observations. The very quiet environment of SOHO, together with the continuity of the observations, enables us to obtain time series of a quality never previously achieved. Our first results confirm broadly what has been found from previous observations: firstly, that the solar irradiance is modulated by the passage of sunspots across the disk, but that not all of the modulation is straightforwardly explained in terms of sunspot flux blocking and facular enhancement, and secondly, that helioseismic inversions are at present more-or-less in agreement with the latest standard solar models. However, we have in addition some new observations that provide hints that profound solar activity is more extensive than its superficial manifestation. This has been obtained partly from a comparison of coarsely resolved measures of radiance with the total irradiance. We also have evidence that magnetic activity plays a significant role in the dynamics of the oscillations beyond its modulation of the resonant frequencies. Pallé *et al* (1990) and Elsworth *et al* (1993) have already shown that the mean linewidths vary with the solar cycle. Comparison of our VIRGO data with IPHIR data reveals that the variation depends on frequency, in a manner that is suggestive of a modulation in the mechanism by which the oscillations interact with the turbulence in the convection zone. Moreover, by comparing the amplitudes of different components of p-mode multiplets, each of which are influenced differently by spatial inhomogeneity, we have found evidence that activity enhances excitation. This appears to be contrary to the temporal variation reported by Pallé *et al* (1990) and Elsworth *et al* (1993), who found that on average mode amplitudes decrease as the global level of activity rises. Further analysis is required to ascertain whether this disaccord is an indication that the excitation process is substantially more complicated than one might suspect or whether the discrepancy is simply a result of the modification of the oscillation eigenfunctions in the solar atmosphere by the magnetic field. Whatever is the case, it is evident that our first results have already raised interesting issues concerning the role played by activity in the global dynamics of the sun.

Acknowledgements

VIRGO is a co-operative effort of many individual scientists and engineers at several institutes in Europe and USA. The VIRGO team is led by Claus Fröhlich (PMOD/WRC, CH) and includes the following co-investigators (in alphabetical order): Bo Andersen (NSC, N), Thierry Appourchaux (SSD-ESTEC NL), Gabrielle Berthomieu (OCAN, F), Dominique Crommelynck (IRMB, B), Werner Däppen (USC, CA USA), Vicente Domingo (SSD/GSFC, USA), Alain Fichot (IRMB, B), Douglas Gough (IoA & DAMTP, GB), Todd Hoeksema (CSSA, Ca USA), Antonio Jiménez (IAC, E), Judit Pap (UCLA, Ca USA), Janine Provost (OCAN, F), Teodoro Roca Cortés (IAC, E), José Romero (PMOD/WRC, CH), Thierry Toutain (OCAN, F), Christoph Wehrli (PMOD/WRC, CH), Richard Willson (Columbia University, NY USA). The VIRGO technical team lead by Hansjörg Roth (PMOD/WRC, CH) was responsible for the successful realization of the experiment and the following inidivuals were involved at PMOD/WRC, Davos, Switzerland: Thomas Fröhlich, Adolf Geisseler, Silvio Koller, Urs Schütz, Jules U. Wyss. at SSD/ESTEC, Noordwijk, The Netherlands: Thierry Beaufort, Jos Fleur, Samuel Lévêque, Didier Martin, Udo Telljohann, at IRMB, Bruxelles, Belgium: André Chevalier, Christian Conscience, Marc Lombaerts, Pierre Malcorps and at IAC, Tenerife, Spain: Maria Gómez, José Herreros. Without the continuous and concerted efforts of the team this experiment would

never have reached the success it demonstrates today.

The VIRGO team has been supported by several national and international funding agencies which are gratefully acknowledged: The PMOD/WRC by the Swiss National Science Foundation under grants 2.860-0.88, 20-28779.90, 20-33941.92, 20-40589.94 and PRODEX, the IRMB by the Fonds de la Recherche Fondamentale Collection d'initiative ministerielle and PRODEX, the SSD/ESA by their annual funds from the Science Directorate, the IAC by the CICYT through PNIE under grants ESP88-0354 and ESP90-0969, the OCA by the CNES and CNRS. Individual contributions to the project have been supported by grants from PPARC of the UK to D. O. Gough, by UCLA under a contract with NASA to J.M.Pap.

Thanks are extended to S.Tomczyk and J.Schou for providing the LOWL data through http://www.hao.ucar.edu/public/research/mlso/LowL/lowl.html and to the Mt.Wilson Observatory for the magnetograms retrieved from the SOHO archive. We have also received help with the inversions from Umin Lee (Tohoku University, Japan).

References

Appourchaux, T., Toutain, T., Telljohan, U., Jiménez, A. and Andersen, B.N.: 1995, *Astr. Astrophys.* **294**, L13.

Appourchaux, T., Andersen, B.N., Fröhlich, C., Jiménez, A., Telljohan, U., Wehrli, C.: 1997, *Solar Phys.* **170**, in press

Balmforth, N.J.: 1992, *MNRAS* **255**, 603

Baudin, F., Gabriel, A. and Gibert, D.: 1994, *Astron.Astrophys.* **285**, L29

Brown, T.M.: 1991, *Ap.J* **0??**, 0??

Chang, H.-Y.: 1995, *Ph.D. dissertation*, University of Cambridge

Crommelynck, D., Fichot, A., Domingo, V., Lee III, R.: 1996, *Geoph.Res.L.* **23**, 2293

Elsworth, Y., Howe, R., Isaak, G.R., McLeod, C.P., Miller, B.A., New, R., Speake, C.C. and Wheeler, S.J.: 1993, *MNRAS* **265**, 888

Friedrich, R.,Fischer, J. and Stock, W.: 1996, *Metrologia* **32**, 509

Fröhlich, C., Romero, J., Roth, H., Wehrli, C., Andersen, B.N., Appourchaux, T., Domingo, V., Telljohann, U., Berthomieu, B., Delache, P., Provost, J., Toutain, T., Crommelynck, D., Chevalier, A., Fichot, A., Däppen, W., Gough, D.O., Hoeksema, T., Jiménez, Gómez, M., Herreros, J., Roca-Cortés, T., Jones, A.R., Pap, J. and Willson, R.C.: 1996, *Solar Phys.* **162**, 101

Fröhlich, C., Crommelynck, D., Chevalier, A., Fichot, A., Finsterle, W., Jiménez, A., Romero, J., Roth, H., Wehrli, C.: 1997, *Solar Phys.* **170**, in press

Harvey, J.: 1985, *ESA SP — would like to get a more accurate ref from BoA* **235**, 199

Kuhn, J.R. and Libbrecht, K.G.: 1991, *ApJ.* **381**, L35

Leifsen, T., Hanssen, A., Andersen, B. N. and Toutain, T.: 1995, *A.S.P. Conf. Ser.* **76**, 520

Neckel, H., Labs, D.: 1984, *Sol.Phys.* **90**, 205

Solar-Gephysical Data: 1996, *Solar-Gephysical Data comprehensive reports* **Number 624, Part II**, 24

Tomczyk, S., Schou, J., Thompson, M.J.: 1996, *ApJ* **448**, L57

Toutain, Th. and Fröhlich, C.: 1992, *Astr. Astrophys.* **257**, 287.

Willson, R.C. and Hudson, H.S.: 1991, *Nature* **351**, 42.